Modeling and simulation of sputter-ion pump performances

Modeling and simulation of sputter-ion pump performances

T. Isoardi*[1], A. Ferretti[1], L. Bonmassar[2], P. Manassero[2]

*Corresponding author: T. Isoardi - tiziano.isoardi@unito.it

[1] *Università degli Studi di Torino*
[2] *Agilent Technologies Italia S.p.A.*

The sputter-ion pump is a capture vacuum pump which operates by sputtering a getter material. Nowadays the most common design is based on a Penning trap. In this work we will study the operating principles of the pump and we will build a model that, starting from design parameters, allows us to simulate its performances. We will consider the ion pumps from Agilent Technologies as a reference for our simulation: the Agilent Diode VIP 40, 55 and 75

1 Introduction

The Penning trap is a device which confines free charged particles (see Fig.1), using an electrostatic-multipolar field combined with a magnetic-dipolar field. The magnetic field confines the ions radially, while the electrostatic field confines them along the axial direction (see Fig.2).
The Penning trap can be used in several applications such as mass spectroscopy, antimatter confinement and studies, quantum computation, ultra-high vacuum generation, etc. In an ion pump the magnetic field (0.1 - 0.2 T) is generated axially to the trap using a permanent magnet. A voltage of few *kV* applied between a cylindrical anode and two titanium cathode plates generates the electric field (see Fig.3 for an example of an ion pump).
The electrostatic field has the form:

$$\bar{E}(x,y,z) = \frac{U_0}{2d^2}(x\hat{e}_x + y\hat{e}_y - 2z\hat{e}_z) \quad (1)$$

where U_0 is the voltage difference between cathodes and anode and d is the trap depth and depends from the geometrical parameters of the trap:

$$d = \sqrt{\frac{1}{2}({z_0}^2 + \frac{{\rho_0}^2}{2})} \quad (2)$$

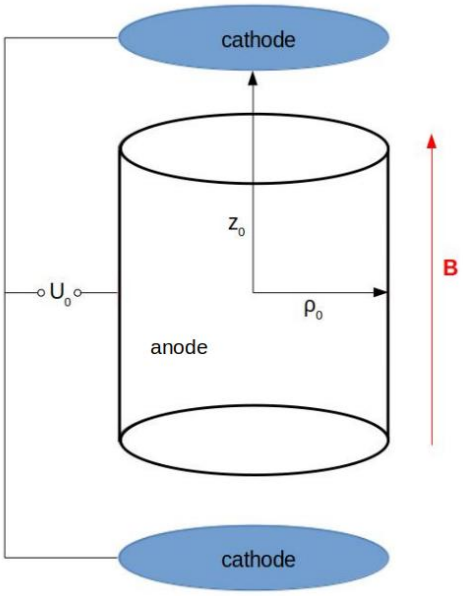

Figure 1: *Example of Penning trap*

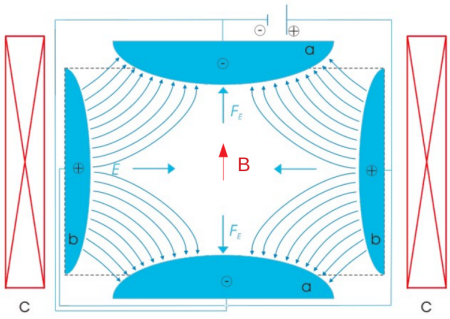

Figure 2: *Electric and magnetic field configuration inside a Penning trap*

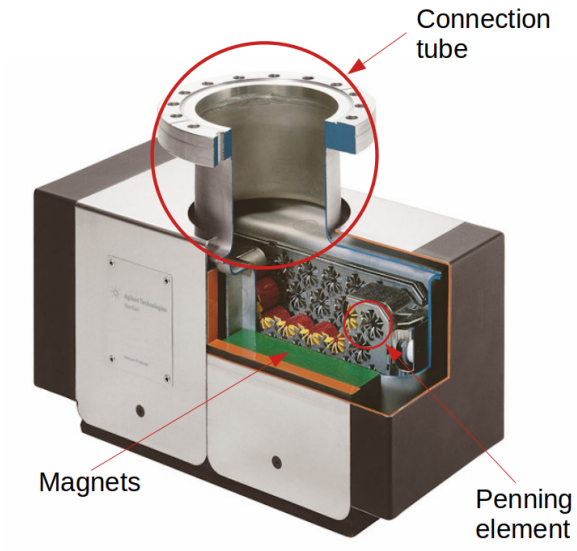

Figure 3: *An example of ion pump*

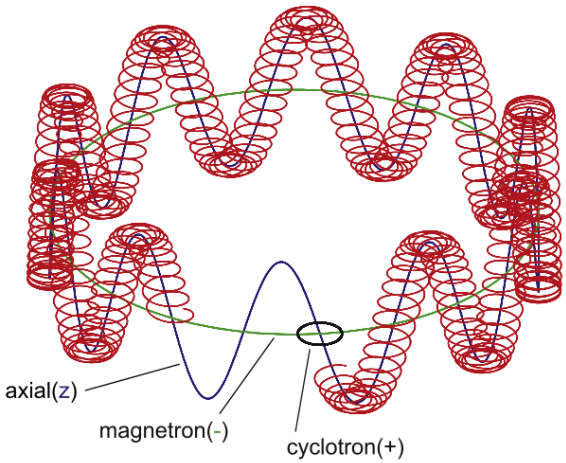

Figure 4: *Trajectory of the trapped particle inside the trap [3]*

where $2z_0$ is the distance between the cathodes and ρ_0 is the radius of the trap. Ion pumps are typically used from pressures of about 10^{-6} *mbar* down to 10^{-10} *mbar*. Electrons originated by field emission from the cathode or by cosmic rays collide with the background gas molecules producing electron-ion pairs. The magnetic and electrostatic field configuration traps the electrons. Within the trap the electrons trajectory is composed by three independent motions each with a specific oscillation frequency (see Fig.4):

- cyclotron motion: the magnetic field generates a Lorentz force that traps the electrons in the radial plane;

$$\omega_+ \simeq \frac{qB}{m} \tag{3}$$

- oscillation along the axis of the trap due to the electric field;

$$\omega_z \simeq \sqrt{\frac{qU_0}{md^2}} \tag{4}$$

- magnetron motion: the combination of electric and magnetic field generates a drift motion in the radial plane

$$\omega_- \simeq \frac{U_0}{2Bd^2} \tag{5}$$

The ions accelerated towards the cathode sputter titanium away from the cathode

forming a getter film on the neighbouring surfaces. The reactive or getterable gas molecules (e.g. CO, CO_2, H_2, N_2, O_2) stick to that film and are buried in the anode. This process removes gas molecules from the trap. Moreover the ion-cathode collisions induce secondary electron emissions from the cathode which are trapped in the pump. These electrons have a high total energy (equal to the potential of the cathode) compared to the ionization energy (about 16 *eV* for nitrogen) that allows them to induce multiple ionizing events. The electrons produced from these ionizations will collide with other gas molecules feeding the process. The trajectory radius of the electrons statistically increase (see Fig.5) with the number of collisions because of the energy loss and the metastability of the magnetron motion (due to the outward radial component of the electric field). This means that, after a certain number of collisions the magnetron radius will become greater than the trap radius and the electrons will be captured from the anode.

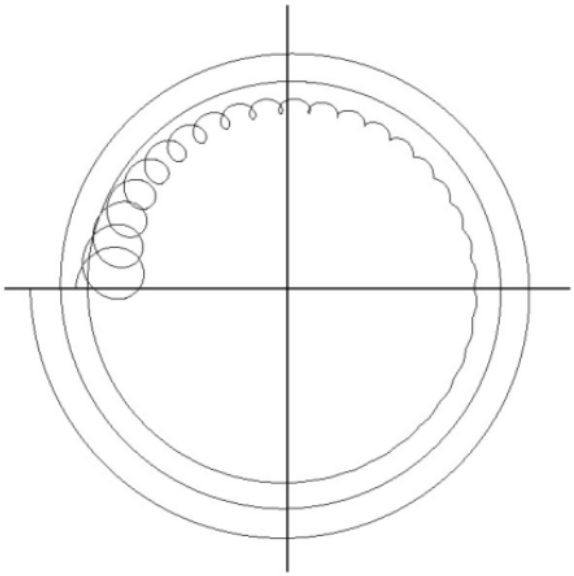

Figure 5: *Increase of the magnetron radius due to the external radial component of the electric field. This effect is more intense when the electron is closer to the anode. The time scale considered is much greater than the magnetron frequency*

After a few tens of milliseconds the electron loss rate becomes equal to the electron generation rate and the current measured between anode and cathode stabilizes. Since the pumping speed is proportional to the relationship between current and pressure, to improve the performance of an ion pump we need to increase the value of the current. In order to do this we developed a simulation to study how the current depends on the trap parameters and settings.
The amplitude of oscillation along the trap axis depends on the kinetic energy of the particles. When the electron energy falls below the ionization threshold they remain trapped in a small volume in the center of the trap giving birth to space charge effects which could limit the total number of active electrons inside the trap. In fact, the presence of many electrons concentrated in a small volume could generate locally an intense electric field capable of deviating them toward the anode. All these processes can be studied in detail by Montecarlo simulations. In particular we started our study using a tool called Simbuca.

2 Simbuca

Simbuca (Simulation of Ion Motion in a Penning trap with realistic BUffer gas collisions and Coulomb interaction using A Graphics Card) [3] is a modular open source tool that allows to simulate the particle behavior inside a Penning trap. This program calculates the particles trajectory for different timesteps taking into account the elastic collisions. These processes require high computing power, so it is not possible to simulate a big number of particles inside the trap. However we decided to use Simbuca (after implementing some algorithms) to understand the phenomena that affect the behavior of individual particles, obtaining a parameterization that

would allow us to extend the simulation to a large number of particles.

2.1 The Hard-Sphere collision model

As previously mentioned the collisions have a key role in understanding the lifetime and the number of ionizations (and therefore the current) of the particles. For the simulation we used the Hard-Sphere collision model.
Changing the cross section we can also evaluate the probability for inelastic collisions and ionizations. The collision probability depends from the mean free path λ.

$$P = 1 - exp(-\frac{v_e \cdot \Delta t}{\lambda}) = \\ = 1 - exp(-\frac{\sigma \cdot p \cdot v_{rel} \cdot \Delta t}{k_b \cdot T}) \quad (6)$$

where v_e is the speed of the electron, v_{rel} is the relative speed between the electron and the neutral molecule, p is the buffer gas pressure, T the temperature and σ is the collision cross-section. This probability is compared in a certain timestep with a random number (RN) generated between 0 and 1. If P>RN a collision occurs: a random uniform number between 0 and 1 is extracted to decide what type of collision has occured (elastic, inelastic or an ionization) considering the energy of the electron and the different total cross-sections. The electron velocity after collision is calculated using total energy conservation and the new direction is chosen using the differential cross section.

2.2 The loss of energy after ionization

Inelastic and elastic collisions occur between electrons and much more massive molecules. So when we consider elastic collision the electron kinetic energy loss is negligible, and there is only a change in direction. On the contrary after inelastic collisions a part of the electron kinetic energy is lost. To calculate this energy loss a random value from a Landau distribution (that govern the loss of energy) is extracted and is subtracted from the kinetic energy of the electron [8]. The Landau distribution is centered around the half of the electron kinetic energy and has a sigma of 10% of this energy. The maximum possible energy loss is equal to the kinetic energy of the electron. If the energy loss extracted from the distribution is bigger than the kinetic energy, the loss value is considered equal to the kinetic energy. An example of Landau distribution is shown in Fig.6. If the collision creates an electron-ion pair the ionization energy is subtracted too.

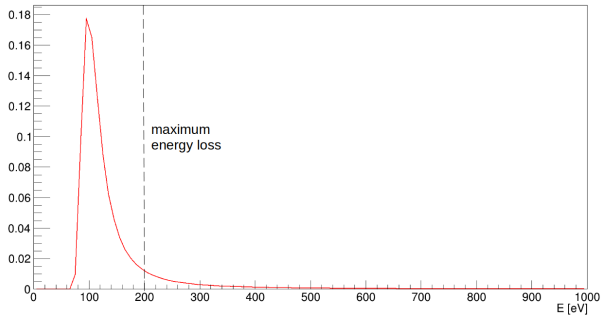

Figure 6: *Example of a Landau distribution centered at the half of the electron kinetic energy that is about 200 eV. In this case this value corresponds to the maximum possible energy loss.*

3 The characteristics of the plasma

After a certain number of collisions the electrons do not have enough energy to ionize the gas molecules and the amplitude of their oscillation along the trap axis is small. As mentioned before this leads to an increase in electron density in a small volume inside the trap leading to the formation of a non-neutral plasma, whose influence on the electrostatic field is not negligible. It is known that there exists a maximum value of density that can be reached in a non-

neutral plasma which is called *Brillouin limit*.

3.1 The Brillouin limit

With the increase of the electrons inside the plasma, the Coulomb repulsive force induces a rotary motion to the plasma that balances the outward forces caused by the non-neutral plasma and centrifugal force [1]. All the radial forces are balanced when the following condition is met:

$$qE_{\mathrm{r}} + qv_\theta B + \frac{m_{\mathrm{e}}{v_\theta}^2}{r} = 0 \qquad (7)$$

where q is the value of a single charge ($1.6{\cdot}10^{-19}$ C), E_r is the radial component of the electric field, m_e is the electron mass, B is the magnitude of magnetic field and v_θ is the rotational velocity. Solving the equation for v_θ and considering that the rate of rotation is ω = -v_θ/r we have:

$$\omega \simeq \frac{\omega_+}{2} \pm \sqrt{\frac{{\omega_+}^2}{4} - \frac{qE_{\mathrm{r}}}{mr}} \qquad (8)$$

The two rotation modes meet when $qE_r/mr=\omega_+^2/4$. In this case we have the Brillouin limit that represents the maximum radial electric field that allows plasma confinement. We can use the Poisson equation to find the relation between the radial electric field and the plasma density n:

$$\frac{1}{r} \cdot \frac{\partial}{\partial r}(rE_{\mathrm{r}}) \simeq \frac{qn}{\epsilon_0} \qquad (9)$$

Solving this equation we can find the maximum density of the plasma:

$$n \simeq \frac{2\epsilon_0 m\omega(\omega_+ - \omega)}{q^2} \qquad (10)$$

$$\Rightarrow n_{\mathrm{B}} \simeq \frac{\epsilon_0 m{\omega_+}^2}{2q^2} = \frac{B^2/(2\mu_0)}{mc^2} \qquad (11)$$

So the maximum density in a non-neutral plasma depends from the magnitude of the magnetic field and from the charged particle mass. For example considering an electron plasma with a magnetic field of *0.1 T* the maximum density is about $5{\cdot}10^{10}$ cm^{-3}.

4 Simulations and results

This section shows the simulation results for a saturated ion pump, i.e. when the pumping effect is due to only the gettering action. The Penning cell diameter is about *20 mm*. The electrostatic field is calculated using a cylindrical geometry of the anode and the open source software openFOAM [13].

4.1 Verification of trajectories with buffer gas

The simulation with background gas can properly reproduce the statistical increase of magnetron radius and the decrease of the oscillation amplitude along the trap axis (see Fig.7 and Fig.8). In these two graphs r and z are respectively the radial distance from the trap axis and oscillation amplitude along the axis.
The single electron is generated with a low magnetron radius (i.e. near the trap axis) and the maximum oscillation amplitude along the axis (i.e. near the cathode). Magnetron radius and oscillation along the axis depend respectively on the radial component of the electric field and on the electron energy. When it is generated, electron velocity is parallel to the cell axis (minimum magnetron radius and maximum oscillation along the axis), but after scattering and loss of energy the radial velocity can increase (increasing magnetron radius) at the expense of a reduction of axial velocity and oscillation amplitude. The axial oscillation amplitude can increase in some points due to the scattering direction which can divert the electron vertically.

4.2 Conservation and loss of energy

Another important step to understand the reliability of the simulation is the analy-

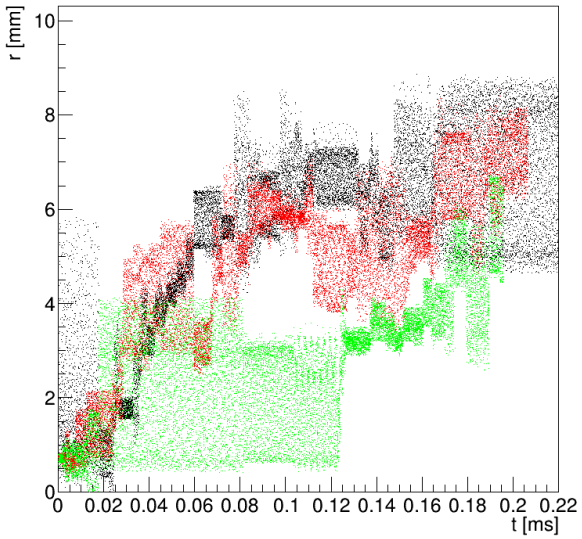

Figure 7: *Radial trajectories of three trapped electrons (trajectories of each electron are represented with different colors). The thickness of the curves along the vertical direction represent the cyclotron radius at a certain time, while the average values of the same thickness are the magnetron radius. In each case, statistically, magnetron radius tend to increase after several collisions with background gas.*

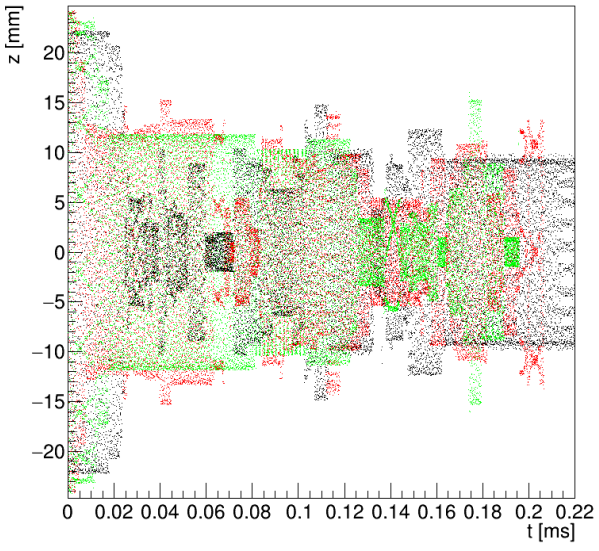

Figure 8: *Axial trajectories of three trapped electrons (trajectories of each electron are represented with different colors). In each case, statistically, oscillation amplitude along the trap axis tend to decrease due to loss of energy after collisions.*

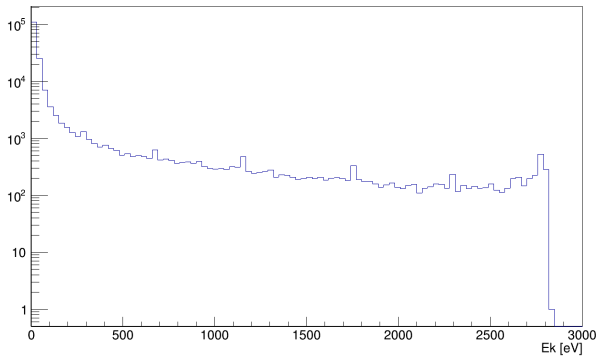

Figure 9: *Electrons kinetic energy distribution: electrons spend a great part of their life with a low kinetic energy because they lose it quickly*

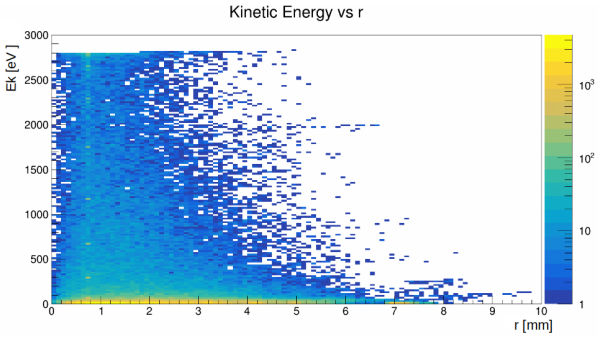

Figure 10: *Variation of the electrons kinetic energy with respect to the radius of the trap*

sis of the kinetic energy evolution, which the electron can achieve. We generated an electron at rest near the cathode (at the potential of *3 keV*) in a trap that contains N_2 at a pressure of 10^{-5} *mbar*. As mentioned before, the loss of energy after the inelastic collisions is extracted from the Landau distribution (see Fig.6). We repeat these simulations 500 times and we sample the kinetic energy of the electrons along their trajectories. Sampling all the electrons kinetic energies of all 500 simulations we obtained Fig.9, Fig.10 and Fig.11. The electrons have maximum kinetic energy when they are in the central plane ($z=0$).

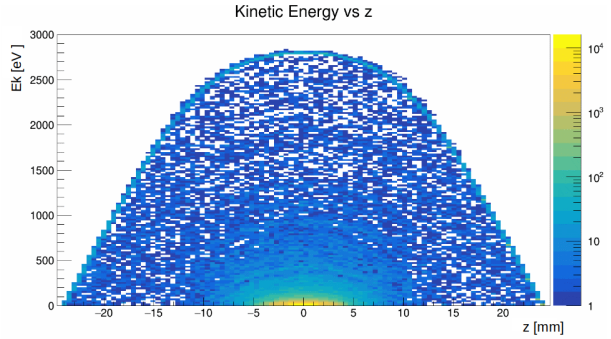

Figure 11: *Variation of the electrons kinetic energy with respect to the axis of the trap. The shape of this distribution derives from the fact that moving away from the central plane (z=0) the kinetic energy is converted into potential energy and vice versa*

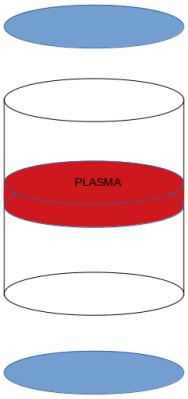

Figure 12: *Plasma model inside the trap*

4.3 Simulation with plasma and calculation of the current-pressure curve

We said that Simbuca requires an high computing power and that the maximum electron density inside the trap is about 10^{10} cm^{-3} due to the Brillouin limit. It is not possible to simulate such a large number of particles when taking into account Coulomb interaction between each particle (2 weeks needed to simulate 128 particles). However we know the following:

- the number of electrons trapped in the Penning cell depends only from the magnetic field and the charge (Brillouin limit);
- we can calculate the electric field for every point inside the trap;
- the electrons with energy lower than the ionization energy have a little oscillation amplitude along the trap axis

So we can make a simulation at the pump working condition (i.e. after the cell has reached the Brillouin limit) by considering a plasma of cylindrical shape with almost the same radius of the cell, centered on the center of the trap and extending for *4 mm* along the axis (see Fig.12). We are aware that this is a raw approximation, but it allows us to calculate in an easy way the effect of the space charge in a Penning cell without significantly changing the parameters that we will need to calculate the current and pumping speed.
Simbuca does not take into account electron-electron collisions which are important when the Penning trap is used as a pump, because when a highly energetic electron passes through the electron plasma, it loses energy through electron-electron collisions. In order to implement this feature we calculate the total and the differential cross-sections using the Moller scattering formula [12]:

$$\sigma \simeq \frac{0.0342}{(E_{\text{cm}}/GeV)^2} mb \qquad (12)$$

$$\frac{\partial\sigma}{\partial\Omega} \simeq \frac{\alpha^2}{{E_{\text{cm}}}^2 sin^4\theta} \cdot (3 + cos^2\theta)^2 \qquad (13)$$

The relevant quantities which influence the behaviour of the pump are the statistical distributions of the time between ionizations, of the lifetime of the electrons inside the trap (i.e. the total time when the electron can ionize) and of the number of ionizations induced by electrons. All of these parameters depend on background gas pressure. To determine these distributions we launch 500 simulations of a single electron generated near one cathode in the presence of plasma and we extract the quantities mentioned above (see Fig.13, Fig.14 and Fig.15). This is repeated for a

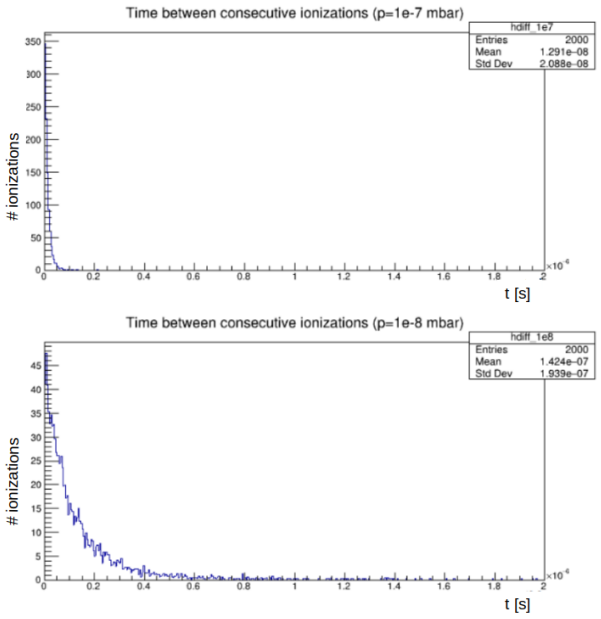

Figure 13: *Time differences between consecutive ionizations at the pressure of 10^{-1} mbar that will be rescaled in 10^{-7} mbar (top) and at the pressure of 10^{-2} mbar that will be rescaled in 10^{-8} mbar (bottom)*

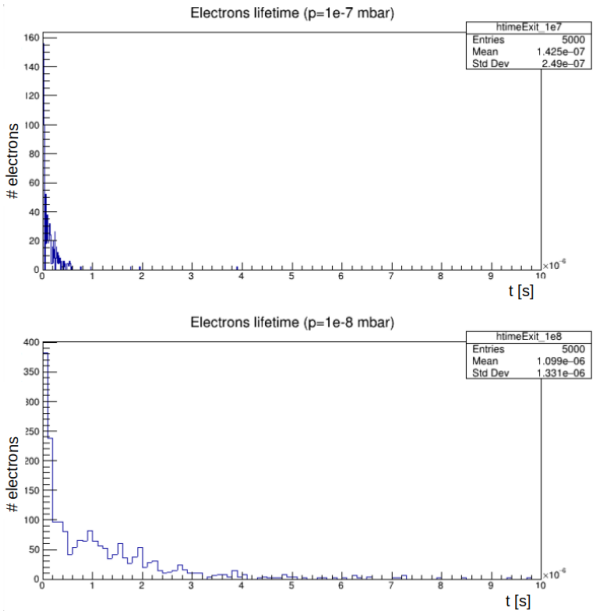

Figure 14: *Lifetimes of the electron at the pressure of 10^{-1} mbar that will be rescaled in 10^{-7} mbar (top) and at the pressure of 10^{-2} mbar that will be rescaled in 10^{-8} mbar (bottom)*

discrete set of pressures values. Actually, simulations are done using a collision probability increased by 6 orders of magnitude (i.e. a pressure and a plasma density 6 orders of magnitude greater) in order to reduce the calculation time, and the results are then rescaled to the correct pressure and density.

Using the data obtained in this way, we build a parameterization which starts from a single electron generated near the cathode. For this electron we do not compute its entire trajectory: instead we extract randomly from the distributions mentioned above the time between ionizations, the total electron lifetime and the number of ionizations during its life. After that we start a timer. When it reaches the ionization time an ionization takes place and an electron-ion pair is generated. The secondary electron is neglected in this first version of simulation because typically it is generated close the trap center, so with a low potential energy and with a low kinetic energy (see Fig.16, Fig.17 and Fig.18), i.e.

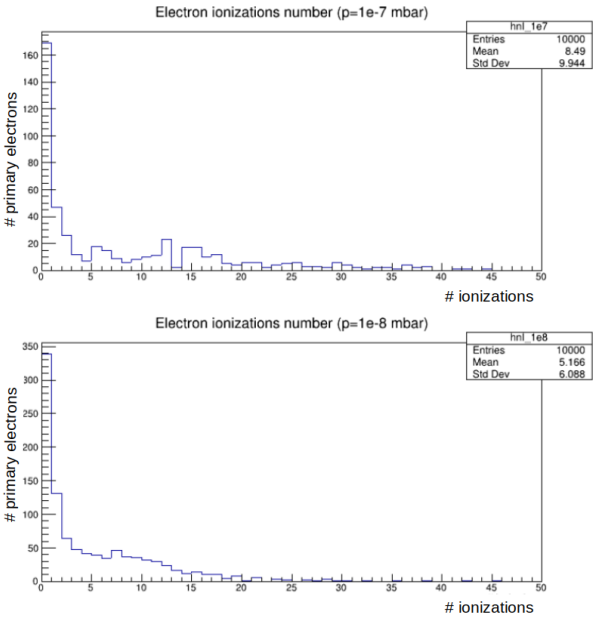

Figure 15: *Number of ionizations for an electron at the pressure of 10^{-1} mbar that will be rescaled in 10^{-7} mbar (top) and at the pressure of 10^{-2} mbar that will be rescaled in 10^{-8} mbar (bottom)*

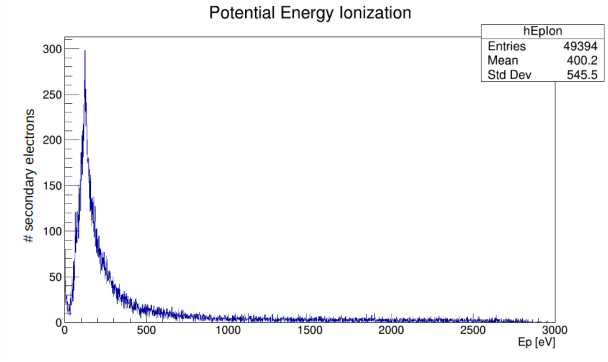

Figure 16: *Potential energy of the electrons generated from ionizations*

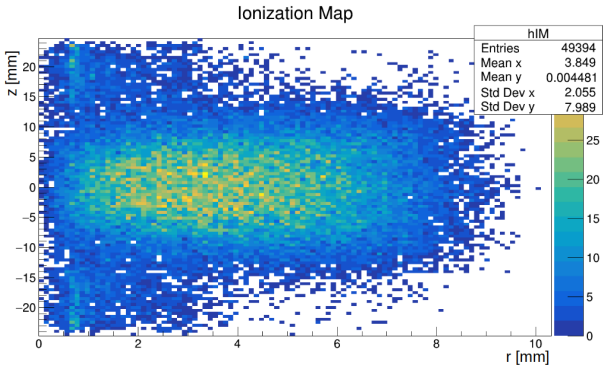

Figure 17: *Ionization map: the electron-ion pairs are generated in the central area of the trap*

unable to make multiple ionization. That's why they are considered to end up in the plasma.
The ion is immediately accelerated towards one cathode where it emits an electron. For this electron we extract time of ionization, lifetime and number of ionizations as for the previous one. Meanwhile the ionization time of the first electron is updated and we reduce by one the number of possible ionizations. So for every timestep and for every electron:

- we compare total time with ionization time;
- we add one more (secondary) electron if an ionization occurs;
- we count the number of ions that collide with the cathode

When the electron performs all possible ionizations or when it reaches its lifetime

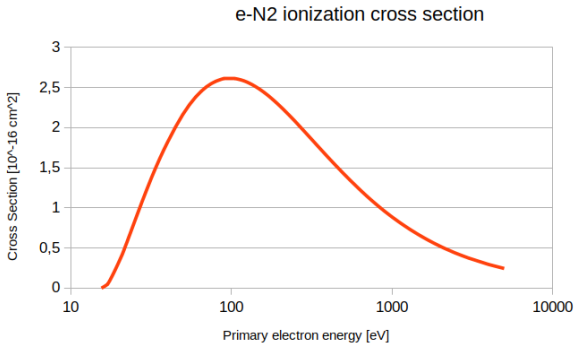

Figure 18: *Ionization e-N_2 cross section: primary electrons with around hundreds eV have large cross-section with respect to more energetic ones [7]*

it is removed from the simulation. So we can study the number of ions that collide with the cathode as a function of the total time and calculate the current at different pressures. Again we can not run a full simulation of current vs pressure curve because of the large number of electrons and ions involved. The approach used is to run the simulation up to the maximum number of ions we can follow in a reasonable amount of time and then extrapolate the information needed. The number of ions produced *N(t)* vs time follow an exponential law:

$$N(t) = N_0 \cdot exp(p_1 t) \qquad (14)$$

where N_0 is the number of initial electrons and p_1 is a function parameter (ionization frequency). Running an exponential fit on the 1000 simulations allows us to make an estimation of the ionization frequency as we can see in Fig.19 and Fig.20.
The maximum number of electrons N_B is defined by the Brillouin limit. If we consider a constant pressure (since it changes in a time scale much larger than the phenomenon we are considering) the current will be:

$$I = qN_B\overline{p_1} \qquad (15)$$

where q is the elementary charge. As said before, the simulations are referred to pres-

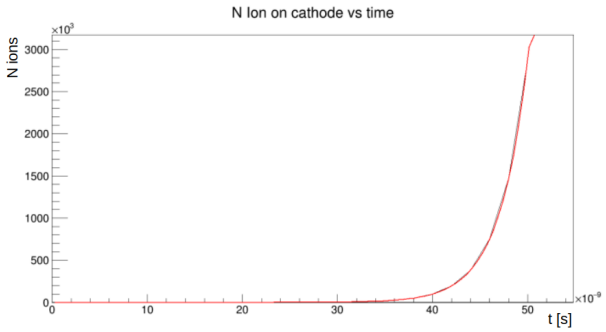

Figure 19: *Number of ions colliding with the cathode vs. time and exponential fitting function*

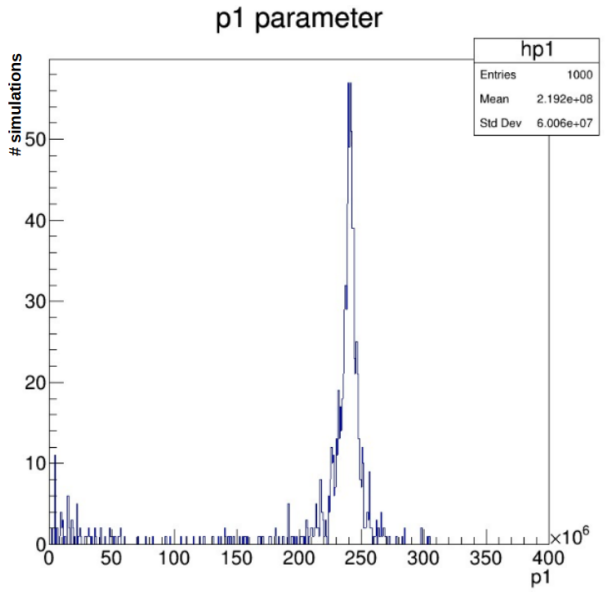

Figure 20: *Parameter p_1 of fitting function of number of ions vs time considering a pressure of $5{\cdot}10^{-1}$mbar (that will be rescaled in $5{\cdot}10^{-7}$mbar)*

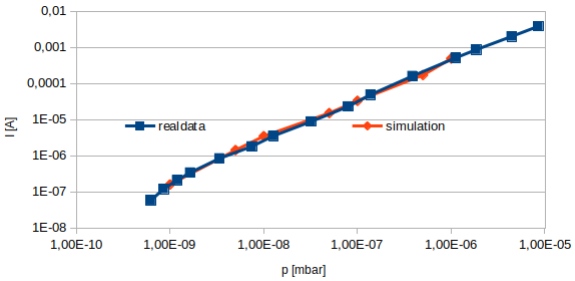

Figure 21: *Current-pressure curve obtained using N_2 as a buffer gas and considering a 40 l/s ion pump*

sures 6 orders of magnitude greater, so to consider the pressures we are concerned with ($p<10^{-6}mbar$), we have to divide the frequency of ionization (p_1) by 10^6.
We repeat this operation for the different pressures values we are interested in and we obtain the current-pressure curve. In our simulations we consider a single cell powered by *3 kV* and using a magnet field of *0.12 T*. As background gas we make a set of simulations using N_2. After obtaining the current as a function of pressure for the single cell we multiply the current values by the number of cells in the ion pump to have a comparison with the experimental data (Fig.21).
The last step is the calculation of the ionization pumping speed (*IPS*) obtained as:

$$IPS = \frac{V}{t} = \frac{N_B R T \overline{p_1}}{p N_A} = k \cdot \frac{I}{p} \qquad (16)$$

In Fig.22 we compare the ionization pumping speed simulated with the pumping speed measured using N_2.

5 Measured pumping speed

As we can see in Fig.22, the measured pumping speed is different from the simulated one. In this section we will analyze the additional parameters that affect the measured pumping speed:

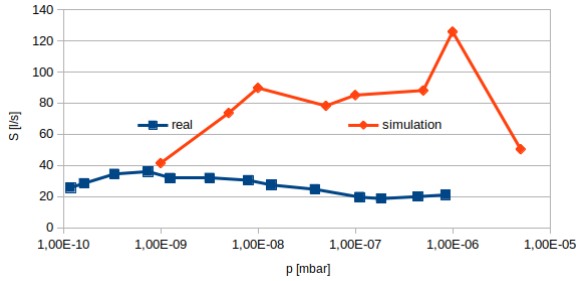

Figure 22: *Pumping speed obtained using N_2 as a buffer gas for a 40 l/s ion pump*

- the conductance of the connecting tube and of the gaps between anode and cathodes
- the sputtering yield
- the sticking coefficient *SC* of the gas species we have to pump

The measured pumping speed (*MPS*) is obtained by:

$$MPS = (\frac{1}{SC \cdot IPS_{\text{eff}}} + \frac{1}{C})^{-1} \qquad (17)$$

5.1 The conductance

In general, in a vacuum system, molecules collide with the walls of the environment and between each other. But if we consider ultra-high vacuum systems (as our system) we can consider as relevant only the collisions with the walls (Knudsen number > 0.5). So the regime to consider for our studies is the free molecular flow. This is an important premise because we know that in this regime the gas conductance of the vacuum system does not depend on pressure, but only on the mean molecular speed and on the vacuum system geometry. So our gas conductance in the connecting tube can be calculated as:

$$C = C'A\tau \qquad (18)$$

where *C'* is the unit surface area conductance and depends from the background gas that we are pumping (see Tab.1 [11]), A is the section of the connecting tube (see Fig.3) and τ is the transmission probability and depends only from the geometry of the connecting tube and in our case can be calculated as:

$$\tau \simeq \frac{1}{1 + \frac{3L}{8R}(1 + \frac{1}{3(1+\frac{L}{7R})})} \qquad (19)$$

where we consider to have a connection tube with a cylindrical shape with an height L and a radius R.

Gas	**H_2**	**He**	**N_2**	**Ar**
C' at 293K [$ls^{-1}cm^{-2}$]	43.86	31.12	11.76	9.85

Table 1: *Conductance per unit area for different gases*

Moreover we have to consider the conductance due to the gap between anode and cathodes which influence pumping speed as:

$$IPS_{\text{eff}} = IPS \cdot \frac{tanh(D)}{D} \qquad (20)$$

$$D = \frac{ka}{7.85\alpha}\sqrt{\frac{IPS}{ab}} \qquad (21)$$

where *a* and *b* are respectively the depth and length of pump unit in cm, α is the gap in cm and *k* is a factor equal to 1 if the pump is open on one side and 0.5 if is open on two sides [4]. In our case we consider *k=1*.

5.2 Sputtering yield

In case of monoatomic metals a semiempirical formula can be used to calculate the sputtering yield that depends from the energy of the incident ion. In particular we used the formula studied by Matsunami et al.[9]

$$Y(E) \simeq 0.42 \frac{\alpha^* Q K s_n(\epsilon)}{U_s[1 + 0.35 U_s s_e(\epsilon)]} [1 - (\frac{E_{th}}{E})^{\frac{1}{2}}]^{2.8} \quad (22)$$

where Y is the sputtering yield; α^*, Q and E_{th} are empirical parameters; U_s is the sublimation energy; $s_n(\epsilon)$ and $s_e(\epsilon)$ are Lindhard's elastic and inelastic reduced stopping cross sections.
To simulate the sputtering yield, when an ion hit the surface of the cathode the Y value is calculated. After that a random number RN between 0 and 1 is extracted from an uniform distribution. If $0<Y<1$ and RN$<Y$ we consider that only a molecule is extracted from the cathode. If $Y>1$ we consider that a first molecule is extracted from the cathode and then we reduce Y by 1. If after this operation we still have $Y>1$ we consider that another molecule is extracted from the cathode and so on. We make this operation until we have $0<Y<1$. When we are in this case we compare Y with a RN and we treat this case as we have seen before. From these simulations we obtain an average sputtering yield of about 0.7. We will use this sputtering value to calculate the sticking coefficient as we will see in the next section.

5.3 Sticking coefficient

The last parameter that we need to calculate the measured pumping speed is the sticking coefficient on Titanium film. It is a function of surface coverage θ that can be calculated using the Langmuir isotherm model. It depends on background gas pressure and sputtering yield of metal atoms that influence the refreshment of film on anode [6]. We can obtain the sticking coefficient as:

$$SC = SC_0(1 - \theta) \quad (23)$$

where SC_0 is the sticking coefficient at zero coverage and θ is the degree of coverage and can be calculated for the monoatomic and diatomic gas respectively as [5, 10]:

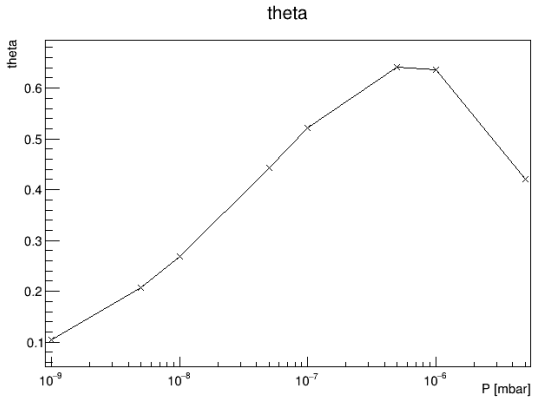

Figure 23: *Degree of coverage at different pressures of Titanium anode from N_2 gas molecules*

$$\theta_{mono} = \frac{Kp}{1 + Kp} \quad (24)$$

$$\theta_{di} = \frac{\sqrt{Kp}}{1 + \sqrt{Kp}} \quad (25)$$

where p is the gas pressure and K is a constant that depends from temperature, activation energy, number of sites per unit area, area, weight of molecule and absorption time.
In this case we have that the total θ depends on the number of free sites that have not absorbed gas molecules and on the sites that are refreshed from sputtered Titanium molecules. Considering this, we have that the degree of coverage of our Titanium anode from N_2 background gas changes with pressure as shown on Fig.23:
In Fig.24, Fig.25, Fig.26 we will see respectively the comparison between the simulation and the real data for three different ion pumps at *3 kV* of voltage and N_2 as background gas. The ion pumps considered are the Agilent Diode VIP 40, 55 and 75.
As we can see the simulation seems to be in good agreement with the real data for the Diode VIP 55 and 75 supplied by *3 kV*. An error of about 20% can be observed for the Diode VIP 40. This major error could arise from the calculation of the conductance as it is the only part that differs from the Diode VIP 55 and 75.

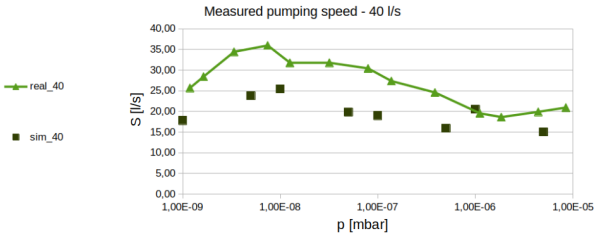

Figure 24: *MPS for a 40 l/s ion pump at 3 kV considering N_2 as background gas*

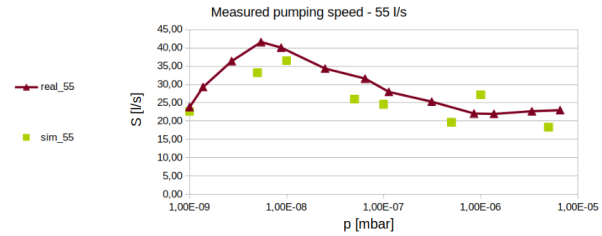

Figure 25: *MPS for a 55 l/s ion pump at 3 kV considering N_2 as background gas*

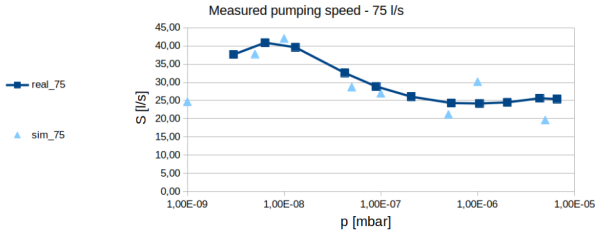

Figure 26: *MPS for a 75 l/s ion pump at 3 kV considering N_2 as background gas*

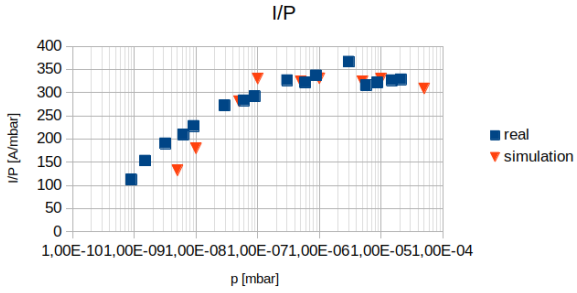

Figure 27: *I/P ratio for an ion pump supplied by 5 kV of voltage*

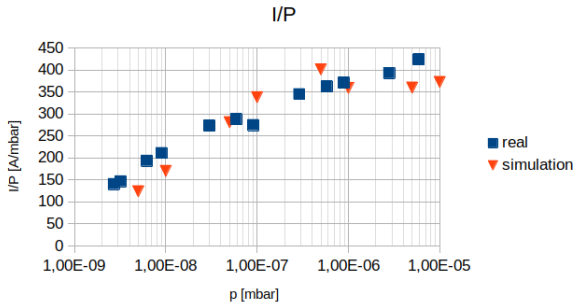

Figure 28: *I/P ratio for an ion pump supplied by 7 kV of voltage*

6 Outlook and conclusions

Some tests are done considering also ion pumps with different voltages and cell diameters. In Fig.27 and Fig.28 are shown the current-pressure ratios (*I/P*) using respectively an ion pump supplied by *5 kV* and *7 kV*.

Presently we calculated only the *I/P* ratios, because to obtain the pumping speed it would be necessary to reconstitute a new experimental set to collect new data. But as we explained before, this ratio is extremely useful to obtain the pumping speed and this is sufficient to understand if the simulation is working well. This model is also used to simulate performances of pumps which have Penning cells with different diameters. In Fig.29 and Fig.30 are reported the *I/P* ratios for pumps with cells diameter respectively of *12 mm* and *24 mm*.

The first results with different cells diame-

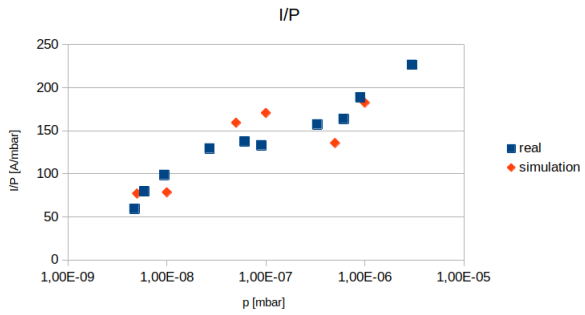

Figure 29: *I/P ratio for an ion pump that have Penning cells with 12 mm of diameter*

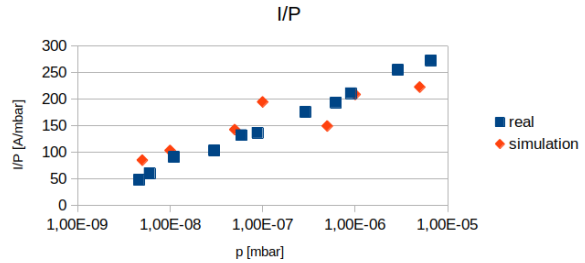

Figure 30: *I/P ratio for an ion pump that have Penning cells with 24 mm of diameter*

ters and supply voltages seem to be promising for what concern the *I/P* ratio. But more studies should be done to investigate if the simulations meet the pumping speed data, taking into account all the parameters previously explained. In fact, at the moment, this model does not pretend to find an optimization of the pump, but only to understand if it is able to predict the experimental data taking into account the physical processes occurring within it. If the next tests will confirm the experimental data, it should be possible to use this simulation to foresee the ion pump performances using different constructive and setting parameters.

7 Summary

In this work we built a model to describe the operation of a real ion pump produced by Agilent Technologies which is currently on the market. This model is able to explain some of the main physics principles that influence the operation of the pump. This is why, since it is based on first principles of physics, it allows us to better study the variations in the behavior of the charges inside the pump as the constructive and setting parameters change.
For our purposes it is useful to divide the pump operation in two time periods:

- from the first electron generation to when the Brillouin limit is reached (order of magnitude of millisecond);
- after the Brillouin limit is reached

As far as the first transient period is very short (milliseconds) for our simulation we considered a constant plasma (both in geometry and in density). From the study of the behaviour of a single electron within the trap (ionization time, energy, lifetime, etc.) we built a parametrization for the evaluation of the ion current at different pressures. To simulate properly the pumping speed we had to include in the model the sputtering yield, the sticking coefficient and the conductance of the connecting tube. The first results obtained for a potential of *3 kV* and for N_2 as buffer gas seem to agree with experimental data for the Diode VIP 55 and 75 while returns an error of about 20% for the Diode VIP 40 which could result from an inaccurate calculation of the conductance. Also simulations with different Penning cells diameters and supply voltages are done obtaining first promising results, but more studies should be done to investigate the reliability of the model with different pump parameters.

List of Figures

References

[1] T. B. Mitchell C. Barnes and M. M. Schauer. “Beyond the Brillouin limit with the Penning Fusion Experiment”. In: *AIP Publishing* (). DOI: http://dx.doi.org/10.1063/1.872276.

[2] R. E. Clausing. “Transactions of the eighth National Vacuum Symposium (American Vacuum Society) combined with the second International Congress on Vacuum Science and Technology (International Organization for Vacuum Science and Technology)”. In: (1961), p. 345.

[3] S. Gorp et al. “Simbuca, using a graphics card to simulate Coulomb interactions in a penning trap”. In: *Nuclear Instruments and Methods in Physics Research Section A: Accelerators, Spectrometers, Detectors and Associated Equipment* 638 (May 2011), pp. 192–200. DOI: 10.1016/j.nima.2010.11.032.

[4] Taekyun Ha and Sukmin Chung. “Optimization of cell geometry for a conventional sputter ion pump by a particle-in-cell simulation”. In: *Journal of Vacuum Science and Technology A* (2009). DOI: https://doi.org/10.1116/1.3106632.

[5] D. J. Harra. “Review of sticking coefficients and sorption capacities of gases on titanium films”. In: *Journal of Vacuum Science and Technology* 13.1 (1976), pp. 471–474. DOI: 10.1116/1.568900.

[6] “Chapter 1.8 - Surface Physics and Its Relation to Vacuum Science”. In: *Handbook of Vacuum Science and Technology*. Ed. by Dorothy M. Hoffman et al. San Diego: Academic Press, 1998, pp. 40–55. ISBN: 978-0-12-352065-4. DOI: https://doi.org/10.1016/B978-012352065-4/50050-X.

[7] Yukikazu Itikawa. “Cross Sections for Electron Collisions with Nitrogen Molecules”. In: *Journal of Physical and Chemical Reference Data* (2005). DOI: https://doi.org/10.1063/1.1937426.

[8] Lev Davidovich Landau. “On the energy loss of fast particles by ionization”. In: *J. Phys.* 8 (1944), pp. 201–205.

[9] N. Matsunami et al. “A semiempirical formula for the energy dependence of the sputtering yield”. In: *Radiation Effects* 57.1-2 (1981), pp. 15–21. DOI: 10.1080/01422448008218676.

[10] R.S. Myong. “Gaseous slip models based on the Langmuir adsorption isotherm”. In: *Physics of fluids* 16.1 (2004). DOI: 10.1063/1.1630799.

[11] Chiggiato Paolo. “Vacuum Technology for Ion Sources”. In: *CAS-CERN Accelerator School: Ion Sources - Proceedings* (Apr. 2014). DOI: 10.5170/CERN-2013-007.463.

[12] Dylan J. Temples. *Elementary Particle Physics in a Nutshell - M. Tully*. 2017.

[13] H.G. Weller et al. “A Tensorial Approach to Computational Continuum Mechanics Using Object Orientated Techniques”. In: *Computers in Physics* 12 (Nov. 1998), pp. 620–631. DOI: 10.1063/1.168744.